Feedback control of canards

Joseph Durham[a] and Jeff Moehlis[b]
Department of Mechanical Engineering, University of California, Santa Barbara, California 93106, USA

(Received 9 January 2007; accepted 11 October 2007; published online 27 March 2008)

We present a control mechanism for tuning a fast-slow dynamical system undergoing a supercritical Hopf bifurcation to be in the canard regime, the tiny parameter window between small and large periodic behavior. Our control strategy uses continuous feedback control via a slow control variable to cause the system to drift on average toward canard orbits. We apply this to tune the FitzHugh-Nagumo model to produce maximal canard orbits. When the controller is improperly configured, periodic or chaotic mixed-mode oscillations are found. We also investigate the effects of noise on this control mechanism. Finally, we demonstrate that a sensor tuned in this way to operate near the canard regime can detect tiny changes in system parameters.
[DOI: 10.1063/1.2804554]

Canards are special periodic orbits that are associated with a dramatic change in amplitude and period due to a very small change in a parameter. Since canards typically exist only for very small regions of parameter space, they are extremely difficult to observe experimentally. In this paper we present a continuous feedback control mechanism that uses only the instantaneous position of the system in phase space to tune the system to be in the canard regime. This involves controlling a slow variable to drift on average toward the canard parameter region, and is inspired by the dynamics of mixed-mode oscillations. A system controlled in this way could serve as a sensor that can detect extremely small changes in system parameters.

I. INTRODUCTION

Canards are periodic orbits for which the trajectory follows both attracting and repelling slow manifolds. They are associated with a dramatic change in amplitude and period over a very narrow interval of a parameter. Canards may be present in singularly perturbed systems of ordinary differential equations: a common scenario in which they arise is that a "small" stable periodic orbit is born in a supercritical Hopf bifurcation and rapidly changes to a "large" relaxation oscillation periodic orbit as a parameter is varied. Canards are the intermediate periodic orbits between the small and large orbits. The shape of these periodic orbits in phase space can resemble a duck; hence the name "canard," the French word for duck. Canards were first found in studies of the van der Pol system,[1–3] and have since been found and analyzed to varying degrees for a variety of chemical, biological, and other systems.[4–22] Because canards typically only exist for very small regions of parameter space, they are extremely difficult to observe experimentally.

In this paper we present a control mechanism that tunes a system to be in the canard regime. This is a continuous feedback control law that uses only the instantaneous position of the system in phase space, and is conceptually similar to one approach used for tuning a system to be at a Hopf bifurcation.[23] Our control mechanism is inspired by the relationship of canards to mixed-mode oscillations (MMOs), which are solutions consisting of sequences of small and large orbits in phase space, as determined by whether the traced orbits are smaller or larger than the corresponding canard solutions. MMOs have been found and analyzed for various systems[24–29] (also see the other articles in this issue). MMO occur, for example, for fast-slow dynamical systems when a variable on average drifts toward and then across a transition from its present state (respectively, tracing a large or small orbit) to a different state (respectively, tracing a small or large orbit). Most commonly, such transitions occur periodically, giving MMOs that can be characterized by the repeating sequence in which the small and large orbits occur, although chaotic MMOs can also occur. Our control mechanism involves a slow variable that similarly drifts toward the canard transition. However, unlike MMOs, by tuning the dynamics of the control variable appropriately, it is possible for the controlled system to converge to the canard behavior, rather than repeatedly switching between a large and small orbit.

A system tuned to be at or near a point in parameter space for which a bifurcation or canard transition occurs can be used to sense parameter changes: one type of behavior indicates the parameter changed in one direction, while another type of behavior indicates the parameter changed in the other direction. For example, suppose a system is tuned to be at a supercritical Hopf bifurcation, as in Fig. 1(a). If the parameter decreases a stable fixed point will be reached, while if the parameter increases a stable periodic orbit will be reached. However, the size of the periodic orbit shrinks to zero as the Hopf bifurcation is approached; if it is difficult to distinguish a fixed point from a small periodic orbit, such a system would have trouble detecting small parameter changes. On the other hand, suppose that a system is tuned to be at a subcritical Hopf bifurcation, with the periodic orbit gaining stability in a saddlenode bifurcation, as in Fig. 1(b).

[a]Electronic mail: joey@engineering.ucsb.edu.
[b]Electronic mail: moehlis@engineering.ucsb.edu.

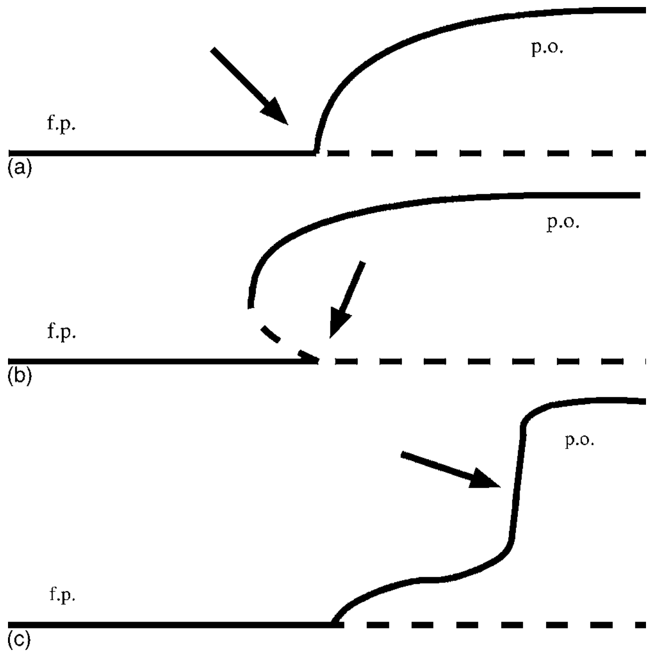

FIG. 1. Bifurcation diagrams showing fixed point (f.p.) and periodic orbit (p.o.) branches for (a) supercritical Hopf bifurcation, (b) subcritical Hopf bifurcation, and (c) canard transition. Solid (dashed) lines indicate stable (unstable) solutions, while the arrows point to the location of the transition. The parameter changes along the horizontal axis, and the vertical axis is a measure of the size of the periodic orbit.

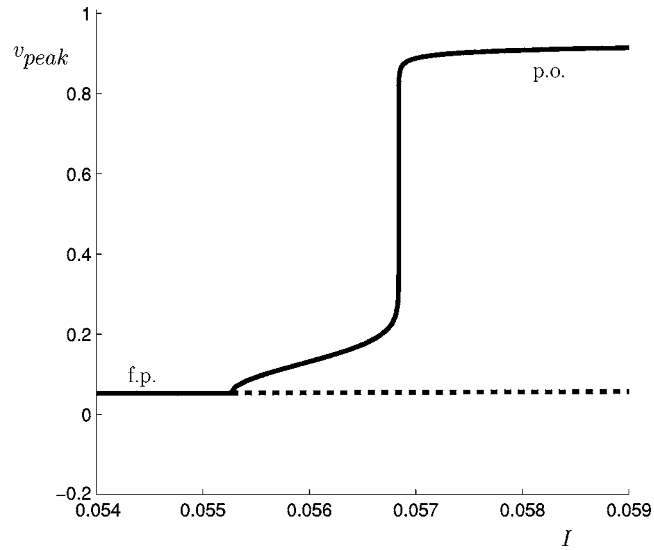

FIG. 2. Bifurcation diagram from simulations of the FHN model, showing a stable fixed point (f.p.) spawning a stable periodic orbit (p.o.) through a supercritical Hopf bifurcation at $I=0.0553$. The size of the periodic orbit is displayed using the maximum value of v along the orbit. A canard transition occurs around $I=0.0568$, where the size of the orbit increases sharply over a very narrow range of I. Solid (dashed) lines represent stable (unstable) solutions.

If the parameter increases even a small amount, a large periodic orbit will be reached, which might be easily distinguished from a stable fixed point. However, such a system would not easily detect a subsequent small decrease in the parameter: hysteresis makes the system stay on the stable periodic orbit branch. In order to "reset" such a sensor, it would be necessary to decrease the parameter by a substantial amount (past the saddlenode bifurcation), then retune the system to be at the subcritical Hopf bifurcation. In contrast, consider a system that is tuned to be at a canard transition near a supercritical Hopf bifurcation, as in Fig. 1(c). The presence of a large periodic orbit indicates a positive change in the parameter, while the presence of a small periodic orbit indicates a negative change in the parameter. Note that, because of the nature of the canard transition, this will be true even for very small changes in the parameters. If it is relatively easy to distinguish a large from a small periodic orbit, such a sensor could detect extremely small parameter changes while avoiding issues with hysteresis. These properties make this final canard scenario a good candidate for sensing tasks. In our present application, we envision using a slow control variable to tune the system to be in the canard regime, then using the system to detect a small change in a system parameter.

In Sec. II, we discuss the presence of canards in the FitzHugh-Nagumo (FHN) model, a prototypical model for neural dynamics that will serve as the example throughout this paper. In Sec. III, we describe the control mechanism that tunes our system to be in the canard regime. Next, in Sec. IV, we determine how well the control works for different parameters in the control law. This includes the result that for certain parameters, the control law leads to MMOs. We also consider this control mechanism for this system subjected to white noise. In Sec. V, we demonstrate how a sensor tuned to operate near the canard regime can detect tiny changes in system parameters. We give concluding thoughts in Sec. VI. While we focus on the FitzHugh-Nagumo equations, we expect that the mechanism that we describe will work for other appropriate systems, provided appropriate tuning of the parameters in the control law is done.

II. CANARDS

The system we consider is the FitzHugh-Nagumo model of neuron spiking behavior.[30–32] The dynamics are described by the differential equations

$$\dot{v} = -w - v(v-1)(v-a) + I \equiv f(v,w;I), \tag{1}$$

$$\dot{w} = \epsilon(v - \gamma w) \equiv \epsilon g(v,w). \tag{2}$$

Here, $\epsilon \ll 1$ is a time-scale separation parameter, and v and w refer to voltage and recovery variables, respectively. Following Brøns,[33] we set $a=0.1$, $\gamma=1$, and $\epsilon=0.008$. The parameter I represents an external current applied to the model, and in this section we treat it as a bifurcation parameter. As shown in Fig. 2, the FHN model with these parameters undergoes a supercritical Hopf bifurcation around $I=0.0553$ and shortly thereafter, the amplitude and shape of the stable periodic orbit change dramatically over a very narrow range of I. This narrow range of I is the canard region: a sample of canard periodic orbits is shown in Fig. 3. For this paper we will consider orbits to be small periodic orbits if they are smaller than orbit (a) and large periodic orbits if they are larger than orbit (e) in Fig. 3.

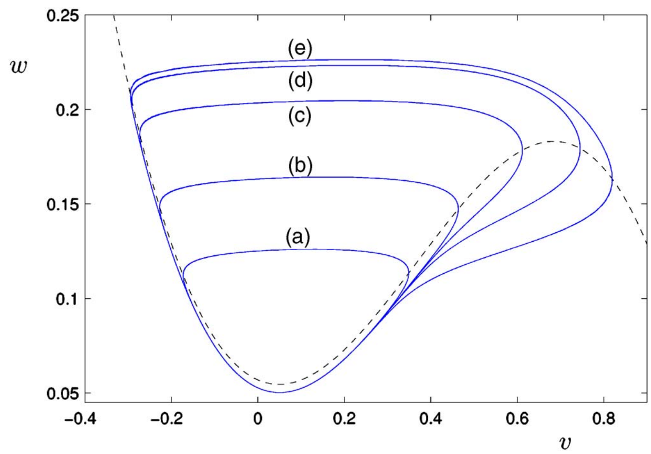

FIG. 3. (Color online) Stable periodic orbit evolution over a small range of parameter I in the FHN model: (a) $I=0.056\,838$, (b) $I=0.056\,838\,45$, (c) $I=0.056\,838\,48$, (d) $I=0.056\,838\,58$, (e) $I=0.056\,84$. Here, and in later phase plane figures, the dashed line is the v-nullcline, where $f(v,w)=0$.

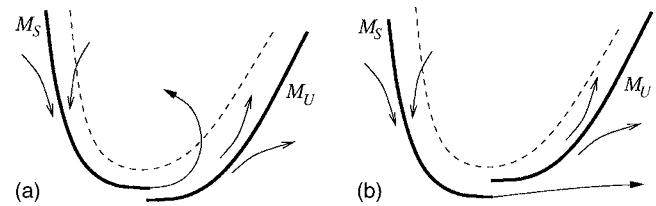

FIG. 4. The two generic situations for the relative positions of the slow manifolds M_S and M_U near the local minimum of the v-nullcline. A trajectory follows M_S, and after passing near the local minimum of the v-nullcline, either (a) returns quickly to a neighborhood of M_S, or (b) undergoes a large excursion before returning to a neighborhood of M_S.

The canard phenomenon can be understood as follows. The system has two nullclines: a cubic v-nullcline, where $f(v,w)=0$, and a linear w-nullcline, where $g(v,w)=0$. If ϵ is set equal to zero, then $\dot{w}=0$ and the v-nullcline is a curve of fixed points and is normally hyperbolic on the pieces for which its slope is bounded away from zero; i.e., away from its local minimum and local maximum when plotted in the (v,w) phase space (see Fig. 3). For $\epsilon=0$, the "left" and "right" parts of the v-nullcline are found to be stable to transverse perturbations, while the "middle" part is found to be unstable to transverse perturbations.

Invariant manifold theorems imply that, for ϵ sufficiently small, invariant manifolds persist within $O(\epsilon)$ of these normally hyperbolic pieces of the v-nullcline, with the manifolds inheriting their normal stability properties from the stability properties of the pieces of the v-nullcline.[34–36] There will thus be a slow manifold M_S, with stable foliation, within $O(\epsilon)$ of the "left" part of the v-nullcline, a different slow manifold, with stable foliation, within $O(\epsilon)$ of the right part of the v-nullcline, and a slow manifold M_U, with unstable foliation, within $O(\epsilon)$ of the middle part of the v-nullcline. The manifolds M_S and M_U can be extended beyond the local minimum and local maximum according to the flow, but the extensions may leave an $O(\epsilon)$ distance of the v-nullcline, and may also lose their normal stability properties.

Generically, the distance between M_S and M_U is nonzero near the local minimum of the v-nullcline. This distance changes as parameters are varied. For the FHN model, a small stable periodic orbit is born in a supercritical Hopf bifurcation, with the manifolds as sketched in Fig. 4(a). As I is increased from the Hopf bifurcation point, the relative position of the manifolds switches to the case sketched in Fig. 4(b). For particular parameters, the manifolds M_S and M_U connect smoothly; for parameters $\mathcal{O}(e^{-K/\epsilon})$ close to this for some $K>0$,[3,12] the periodic orbit is called a canard, and it follows M_U for a substantial distance.

Singular perturbation theory can be used to predict the parameter values at which these manifolds connect.[7,15,19] Of particular utility, Eqs. (3.10) and (3.23) of Brøns[19] predict the Hopf bifurcation point (I_H in our notation below) and canard point (I_C in our notation below), respectively. Since functions f and g in Eqs. (1) and (2) have no dependence on ϵ, Brøns' equations in our notation simplify to

$$a_1 = -\frac{1}{16}(f_{vv}^2 g_w + g_v f_w f_{vvv}), \tag{3}$$

$$\delta = \frac{f_{vv} g_w f_I}{g_v f_w}, \tag{4}$$

$$I_H(\epsilon) = I_{\text{base}} - \frac{g_w g_v f_w}{\delta g_v f_w}\epsilon + O(\epsilon^2), \tag{5}$$

$$I_C(\epsilon) = I_H(\epsilon) - \frac{8a_1}{f_{vv}^2 \delta}\epsilon + O(\epsilon^2). \tag{6}$$

Here, I_{base} is the parameter value at which the w-nullcline intersects the v-nullcline at its local minimum, and the derivatives are evaluated at this intersection in phase space. For our system (1) and (2), this intersection occurs at

$$v_i = (1 + a - \sqrt{1 - a + a^2})/3 \approx 0.048\,687, \tag{7}$$

$$w_i = v_i/\gamma \approx 0.048\,687, \tag{8}$$

$$I_{\text{base}} = \frac{v_i - 2v_i^2 + v_i w_i - 2v_i^2 w_i + v_i^2 w_i}{\gamma - 2w_i} \approx 0.051\,064, \tag{9}$$

and this theory predicts that the Hopf bifurcation point and canard point will occur at $I_H \approx 0.0553$ and $I_C \approx 0.0566$, respectively. Both of these results are accurate to first order in ϵ, and match the numerical results shown in Fig. 2 to that order.

III. CONTROL METHOD

Our goal is to design a control mechanism that steers the FHN model to the canard regime, without precise foreknowledge of where this occurs in parameter space. Since I is a natural bifurcation parameter in Eqs. (1) and (2), it makes a natural control variable as well. We will choose the control law so that I evolves slowly enough that the behavior for an instantaneous (but slowly changing) value of I can be well approximated by that predicted from Fig. 2 for constant I. If the dynamics are (approximately) those of a large periodic orbit, I should then be decreased, and if the dynamics are (approximately) those of a small periodic orbit, I should be increased. If the changes in I cause it to drift back and forth across the canard region, this strategy would produce MMOs. However, when properly tuned, as described below, it will converge to the intermediate canard orbits.

We choose to use continuous feedback control based on the position of the system in phase space, similar to the approach of Moreau and Sontag for tuning to a Hopf bifurcation.[23] The local minimum of the v-nullcline is the base point for our measurements and we construct a control circle around this point to determine whether trajectories are instantaneously on a small or large orbit. Specifically, we will assume that a trajectory outside the control circle is (approximately) on a large periodic orbit, and I should be decreased. On the other hand, a trajectory inside the control circle is assumed to (approximately) be on a small periodic orbit, and I should be increased. While this identification is not always correct (for example, large periodic orbits spend some time within the control circle), we show below that under proper tuning, I will cycle over a small range, with a corresponding canardlike trajectory that balances the effects of sometimes being inside and sometimes outside the control circle.

To include this control strategy in the FHN model, we augment Eqs. (1) and (2) with the following differential equation for I:

$$\dot{I} = c(r_0 - r). \tag{10}$$

The new variable $r=\sqrt{(v-v_i)^2+(w-w_i)^2}$ is the instantaneous Euclidean distance from the local minimum of the v-nullcline. The parameters c and r_0 determine the control strength and radius of the control circle, respectively, and will be tuned as described in the next section to produce a "good" canard. This control strategy is memoryless, as it depends only on the instantaneous position in phase space, and also does not require foreknowledge of the parameter values for which canards exist. That being said, it is only expected to work for fast-slow systems near a supercritical Hopf bifurcation, where the system must begin in an oscillatory region of parameter space but can start with the control variable on either side of the canard point. This control strategy also requires approximate knowledge of the size of periodic orbits on either side of the canard point to pick an initial value for r_0. For the present application, setting r_0 to one third of the distance from the local minimum of the v-nullcline to the local maximum is a reasonable starting point as it approximately balances the amount of time trajectories near the canard region spend inside versus outside the control circle.

IV. TUNING TO THE CANARD REGIME

To compare the effectiveness of this control strategy for various values of c and r_0, we would like to measure the distance over which the trajectory remains in the neighborhood of the slow manifold M_U. This manifold is within $O(\epsilon)$ of the middle portion of the v-nullcline. This implies that the slope of M_U must be close to that of v-nullcline. When a trajectory departs from a neighborhood of M_U, it does so abruptly, making a sharp turn with a large change in slope.

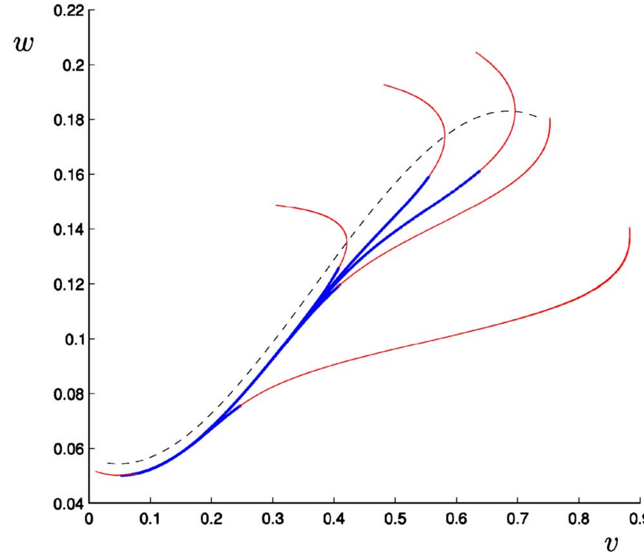

FIG. 5. (Color online) Demonstration of how our distance measure classifies several trajectories. The dashed line is the v-nullcline, with $O(\epsilon)$ of M_U. The thicker blue part of the trajectories count towards the distance following M_U; the thinner red pieces do not. Here, the longest distance is approximately 0.6 and the shortest 0.15.

With these considerations in mind, our distance measurement begins when the trajectory passes the local minimum of the v-nullcline. We consider the trajectory to have departed the neighborhood of M_U when its slope differs by 0.09 from that of the v-nullcline with the same value of v. This value, which is an order of magnitude larger than ϵ, was chosen so that the trajectory with the longest measurement has a large change in slope just before the local maximum of the v-nullcline. Fig. 5 shows several trajectories and how our method classifies their distance. We emphasize that this distance measure is only used for diagnostic purposes; it is not used in the control law itself.

The results of a two-parameter study of c and r_0 using this distance measure are shown in Fig. 6, where we average over multiple visits near M_U to account for the possibility of MMOs (see below). Using other values for this slope difference threshold results in a slightly different specific largest canard, but the results are very similar. As r_0 increases from 0.15, the distance over which trajectories remain in the neighborhood of M_U generally increases until reaching its peak around $r_0=0.234$. The longest canard orbit in our study occurs for $c=10^{-8}$ and $r_0=0.234$, and is shown in Fig. 7; we will refer to this as the maximal canard. Just above this value of r_0, the length of trajectories drops sharply as the trajectories turn off a shorter distance up M_U. As the two-parameter study shows, using a smaller value of c produces longer tracking of M_U and thus more canardlike shapes. Using values of c less than 10^{-8} does not significantly improve the distance measure.

The value of c must be smaller than 10^{-4} to tune the system to the canard region. As demonstrated in Fig. 3, the size of the canard region in I is smaller than 10^{-5}, with maximal canards in a range of I several orders of magnitude smaller. Our choice of memoryless, continuous control also mandates very small corrections. This size constraint on c

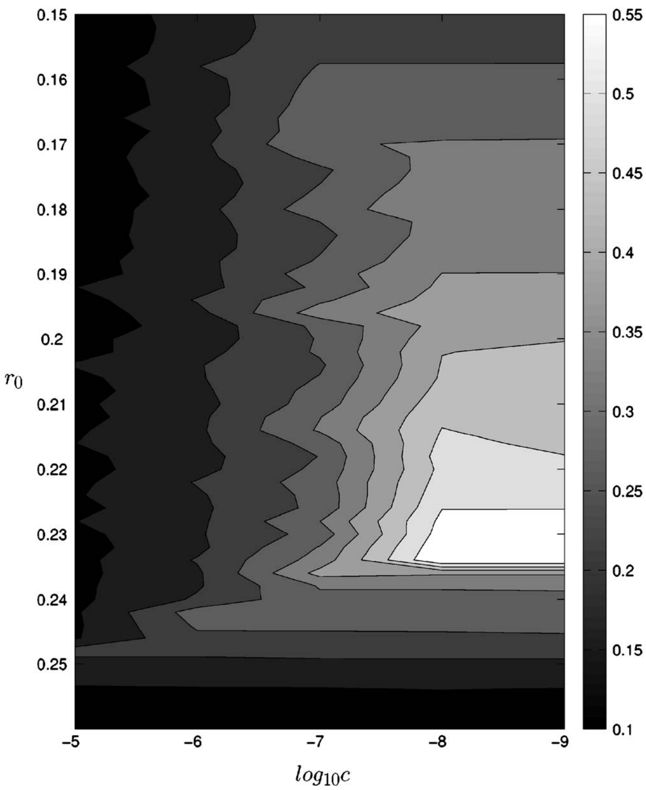

FIG. 6. Contour plot of the average distance the trajectories remain in the neighborhood of M_U after transients have died out. Average is taken over at least 40 successive visits near M_U.

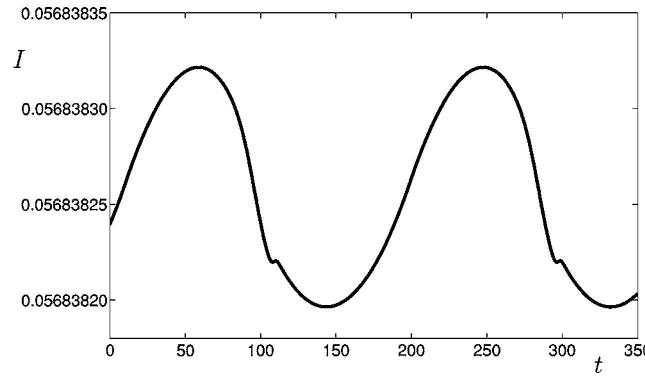

FIG. 8. Evolution of I for the trajectory in Fig. 7.

effectively creates three time scales for the system (1), (2), and (10), as $1 \gg \epsilon \gg c$. Over the maximal canard trajectory, the control variable I is never stationary but enters into a repeating cycle, as shown in Fig. 8. As the trajectory passes near the local minimum of the v-nullcline, it is in the center of the control circle and I increases most rapidly. The trajectory then passes out of the circle on its way up M_U, and I starts to decrease more rapidly as the orbit moves through the canard's "head." On its return to M_S, the trajectory briefly passes through the top of the control circle, resulting in the short reversal in Fig. 8. As this occurs away from the v-nullcline, the trajectory is moving quite rapidly, keeping the reversal small.

While the canard trajectory shown in Fig. 7 traces a single orbit each time around, this is not always the case. For $c=10^{-8}$, we also found MMOs with one large and one small orbit, as shown in Fig. 9. These MMOs occur when the control strategy overcorrects for the value of I. When the trajectory departs the local minimum of the v-nullcline headed for a large orbit, it spends a substantial amount of time outside the control circle, which lowers the value of I. When the trajectory re-enters the control circle, I begins to increase again. If the control circle is too small and/or the control strength c too large, then when the trajectory departs again it will have overcorrected the value of I, leading to a small orbit. The trajectory then spends a substantial amount of time inside the control circle, which increases the value of I, and can lead to another large orbit.

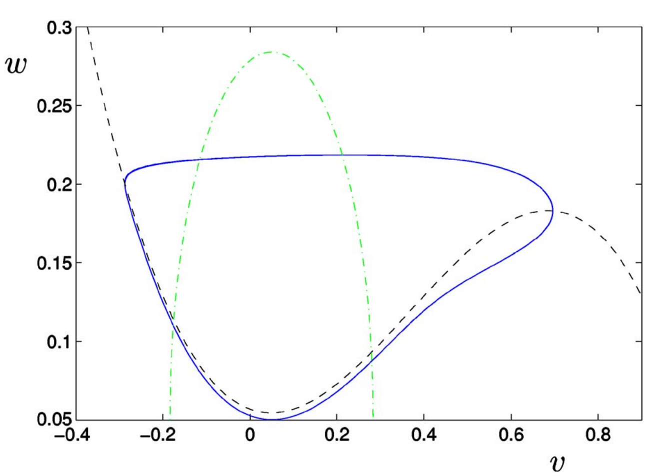

FIG. 7. (Color online) This canard trajectory, produced using control with $c=10^{-8}$ and $r_0=0.234$, has the longest distance measure along M_U. The axes are not square, so the dot-dashed control circle appears elliptical.

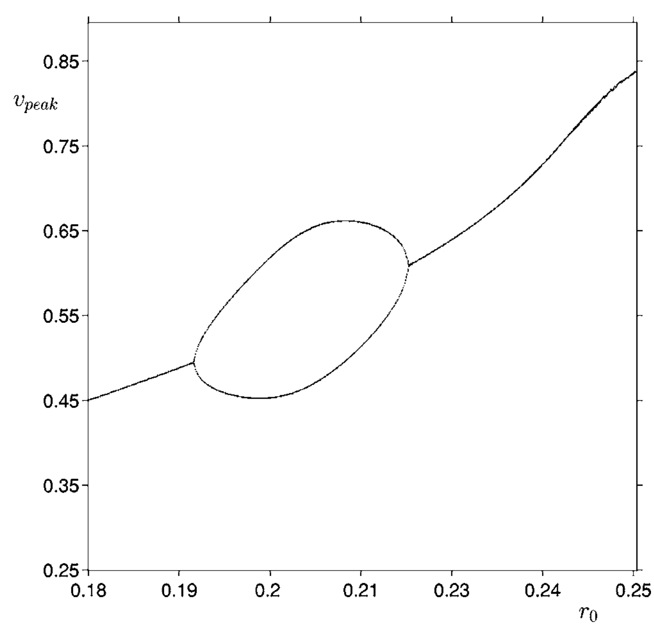

FIG. 9. Bifurcation diagram for $c=10^{-8}$ showing peak values of v, generated by adiabatically increasing the value of r_0, omitting transients. There is a period-2 bubble corresponding to a MMO with one small and one large orbit as r is swept from 0.18 to 0.25. The maximal canard has $v_{\text{peak}} \approx 0.65$.

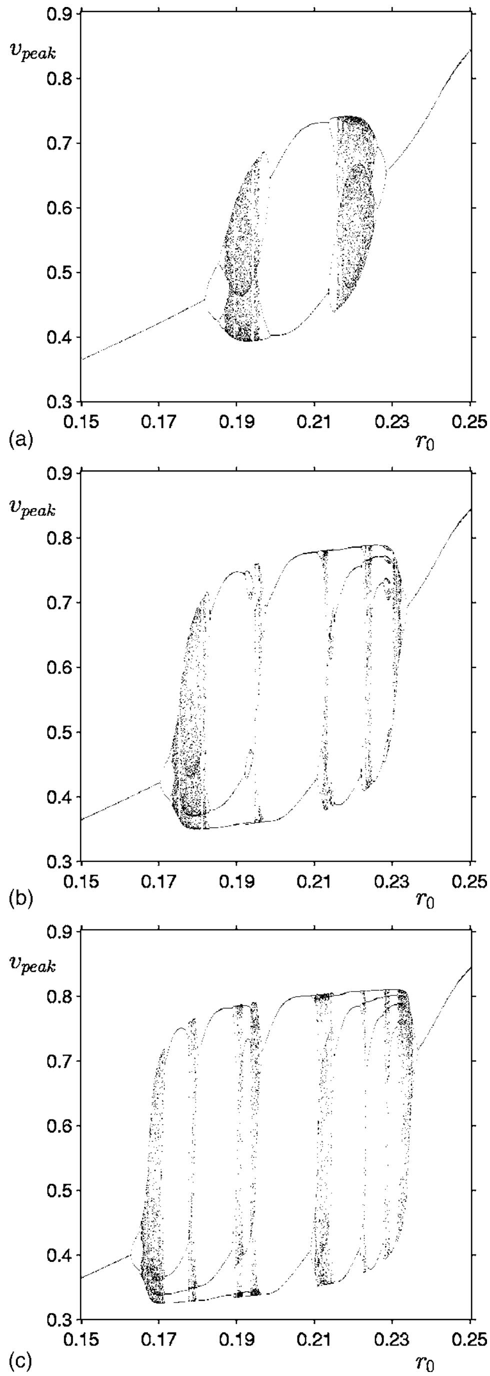

FIG. 10. Bifurcation diagram, as in Fig. 9, for (a) $c=2\times10^{-8}$, (b) $c=5\times10^{-8}$, and (c) $c=10^{-7}$, all showing period-doubling cascades to chaos and various periodic windows corresponding to periodic MMOs. The maximal canard has $v_{\text{peak}}\approx0.65$.

When c is increased, the window of MMOs expands. Figure 10 shows bifurcation diagrams for $c=2\times10^{-8}$, 5×10^{-8}, and 1×10^{-7}. For all three of these, the period-doubling "bubble" in Fig. 9 expands into cascades of period-doubling bifurcations, that leads to chaotic MMOs. As c increases, the width of the region with complex behavior broadens as the propensity for overcorrection in I increases. The chaotic region is broken up by windows of MMO periodic orbits, with the number of MMO windows increasing with c. Each of these windows corresponds to a different

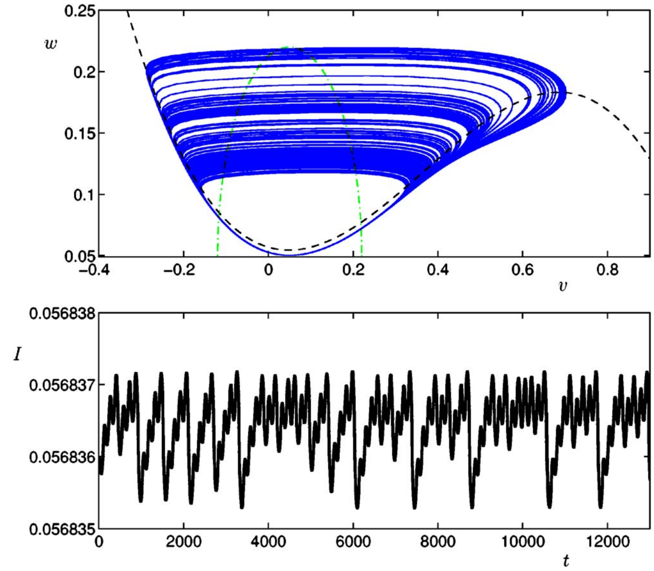

FIG. 11. (Color online) Control with $c=10^{-7}$ and $r_0=0.17$ produces chaotic MMOs.

type of MMO, beginning with 1^n orbits (L^s means s small orbits for every L large orbits) for small values of r_0, transitioning through 1^1 in the middle of the chaotic region, and ending as n^1 orbits, as can be seen best in Fig. 10(c). The same chaotic MMO bifurcation structure has been observed experimentally for the Belousov-Zhabotinski reaction,[37] as well as an electrochemical system.[38] These results are also very reminiscent of results of Petrov *et al.*[24] Other chaotic MMOs reported recently have a more classical period-doubling cascade bifurcation structure, and can be interestingly interpreted as spikes triggered by a chaotic background.[22]

Figure 11 shows the chaotic trajectory for $c=10^{-7}$ and $r_0=0.17$ with the associated time series for I. In Fig. 12, the

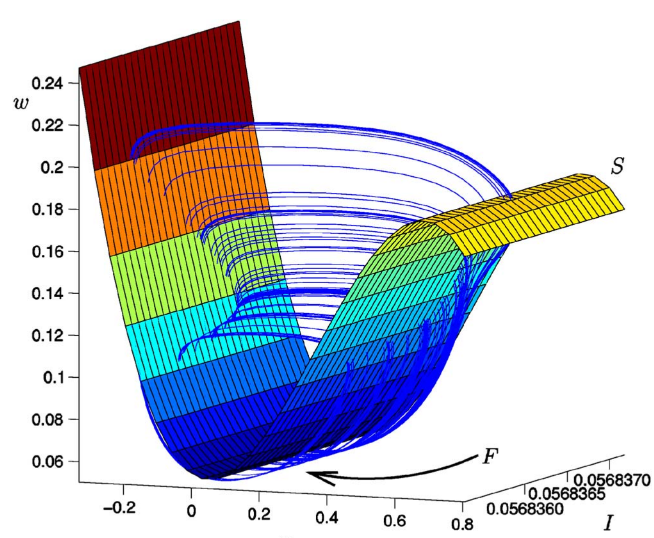

FIG. 12. (Color online) Three-dimensional representation of the chaotic trajectory from Fig. 11, with the (v,w)-phase plane augmented with a dimension for I. The cubic v-nullcline is now the two-dimensional surface S with fold-line F.

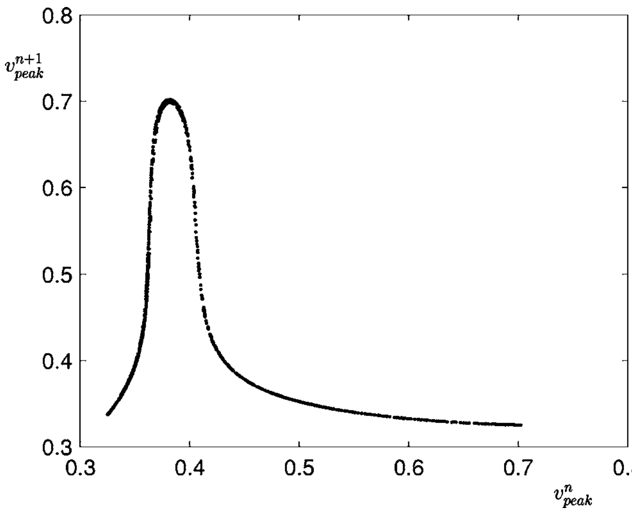

FIG. 13. Map of peak value of v in Fig. 11 vs the previous peak. This one-dimensional map shows that the spread of orbits in Fig. 11 is due to chaos.

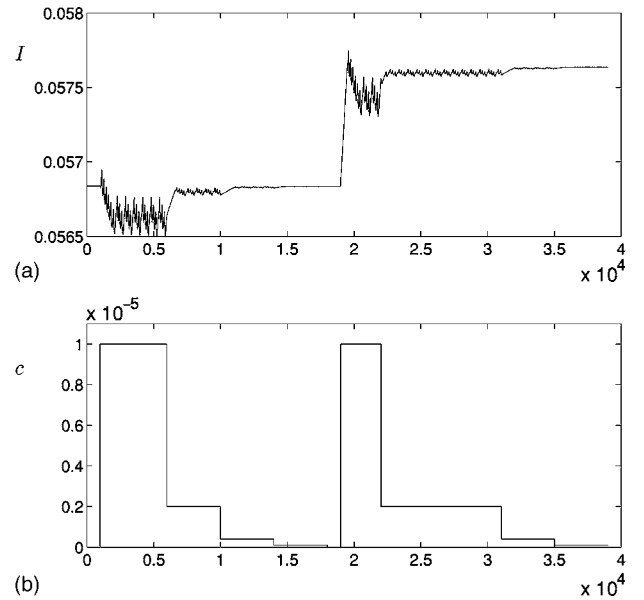

FIG. 14. (a) The control variable I first locates the initial canard window for γ=1.0. After it achieves a lock, γ is reduced to 0.985 and I then tunes to the new canard window at I=0.057 64, as confirmed by simulations. (b) The control strength c is varied based on recent history of I, as described in the text.

(v,w)-phase plane is expanded with a third dimension for the control variable I, creating a three-dimensional view of the chaotic trajectory in Fig. 11. The v-nullcline is expanded into the I-dimension to form a two-dimensional folded surface S, with the line of local minima of the v-nullcline now referred to as the fold-line F. This chaotic behavior is not the product of integration error or other noise, as a map from the max value of v from one orbit to the next is distinctly one dimensional, as shown in Fig. 13.

We also studied the effects of moving the control circle so it was not centered on the local minimum of the v-nullcline. The control strategy still functions when the circle is displaced by less than half of r_0. These results indicate that the control strategy is effective without precise positioning of the circle, although the specific end canard or MMO behavior does change when the circle moves. However, if the circle is displaced so it no longer contains the local minimum of the v-nullcline, the controller cannot work.

Our control method is robust to large, but infrequent, changes in system properties. For the FHN model, we use steps in γ to simulate these sudden changes. As shown in Fig. 14(a), the control method is capable of responding to these changes and locating the new canard region. The time it takes the system to reach the canard window depends on the value of c, with larger values locating the canard window more quickly and smaller values finding it more precisely. To reach the canard region both quickly and precisely, we developed a strategy for adjusting c depending on the past history of I. Essentially, if I has settled in and keeps oscillating over the same region, c is reduced to more accurately determine the canard window, as shown in Fig. 14(b). If I is moving in one direction for a sufficiently long time, c is increased to reduce the time until the new canard window is acquired. These determinations of the trend of I are made by examining the behavior of I over the last 20 orbits. If the difference between the average value of I for first five orbits and the last five orbits is significantly smaller than the standard deviation of I over the orbits, we consider I to have settled in and reduce c to locate the canard window more precisely. Conversely, if the change in the average value of I is an order of magnitude greater than the standard deviation, c is increased to decrease the settling time. This adaptation of c requires knowledge of past values of I, but greatly improves the settling time for smaller values of c. In addition, this adaptation mechanism allows for rapid, precise convergence to the canard region from an initial condition.

The high precision required to achieve tuning to a specific canard orbit raises the question of whether the method will work in the presence of noise. One potential source of noise for the FHN neuron model is a noisy external current, which would directly affect the v equation. Considering Gaussian white noise, Eqs. (1), (2), and (10) are rewritten

$$\dot{v} = -w - v(v-1)(v-a) + I + \sqrt{2D}\,\eta(t), \tag{11}$$

$$\dot{w} = \epsilon(v - \gamma w), \tag{12}$$

$$\dot{I} = c(r_0 - r), \tag{13}$$

where $\eta(t)$ represents Gaussian delta-correlated noise with zero mean and unit variance that enters the system continuously. To simulate the response of our controlled FHN model to this noise, we use a fourth-order Runge-Kutta method adapted for noise.[39]

Under this type of noise, our controller is able to approach I values close to the canard transition, but is unable to produce repeated canard-shaped orbits. Figure 15 shows what happens to the maximal canard in Fig. 7 when a small amount of noise is injected. To achieve a canard shape, the trajectory must follow M_U. Even small amplitudes of white noise cause the trajectory to depart from M_U and the control logic is simply not set up to offset these local effects. Instead

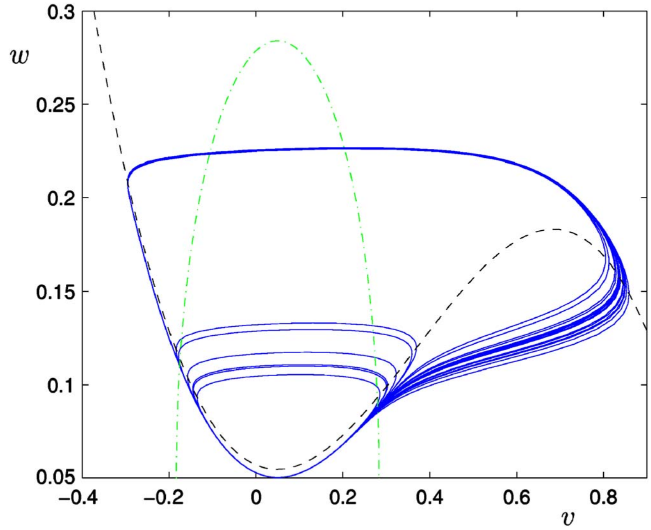

FIG. 15. (Color online) Noisy MMO produced using $c=10^{-8}$, $r_0=0.234$ and noise strength $D=10^{-11}$. This is the same controller that produced the maximal canard in Fig. 7. With noise, the controller can only find the general location of the canard window; the continuous noise precludes repeated canard trajectories.

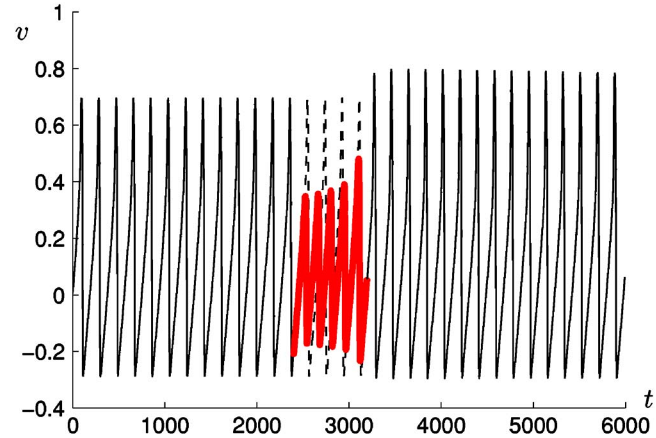

FIG. 16. (Color online) Here the control parameters are chosen as in Fig. 7 (i.e., $r_0=0.234$ and $c=10^{-8}$) so that the system initially traces out the maximal canard trajectory, as shown by the thin black line up to $t=2500$. The thick, red lines in the middle of the figure show that the system responds by tracing out small periodic orbits when γ is decreased by 1×10^{-5} from its original value $\gamma=1$. This is to be compared with the dashed lines which correspond to how the time series would have evolved had γ not changed. After γ returns to its original value, the system evolves according to the thin black line. The control will slowly retune the system to the maximal canard trajectory.

of canard shapes, Eqs. (11)–(13) produce noisy MMOs even for tiny noise strengths. For our system, larger (smaller) values of noise strength D move the fork in Fig. 15 lower (higher) on M_U. Note that it is possible to produce similar results to those from previous studies of noise-induced spiking[14,18] using our method: choose a small value for r_0 (say, 0.12) and, in the absence of noise, the control will produce small periodic orbits; with noise, the system will sporadically produce large orbits.

To tune to maximal canard orbits in the presence of noise, perhaps an alternative control method could be developed based on deviation of the orbit from M_U. This would have the potential to overcome continuous noise, but would require either specific prior information about the canard system or an adaptive memory.

While the control circle method cannot produce repeated canard shaped trajectories in the presence of noise, it does tune the system to be close to the canard transition. When the system is operating near the canard regime, it is still sensitive to changes in system properties and can detect them, as we will now show.

V. SENSING

We now suppose that the control method described above is being used to tune the system to be near the canard regime. We will demonstrate with several examples that such a system can be used to rapidly detect a very small change in the system parameter γ. This relies on the fact that even rather small perturbations to system properties shift the position of the canard transition so that the system will produce only small or large periodic orbits, which can then be distinguished from the system's behavior in the canard regime.

First, consider the control parameters $r_0=0.234$ and $c=10^{-8}$, which give the maximal canard trajectory in the sense of maximizing the distance over which the trajectory is close to M_U (see Fig. 7). When γ is decreased by one part in 100 000, the trajectory immediately begins tracing out a small periodic orbit, which can be easily distinguished from the canard orbit (see Fig. 16). After γ is restored to its original value, the system slowly returns to tracing out the maximal canard trajectory. There are no issues with hysteresis associated with this return.

Even when the system is not tuned to give the maximal canard, it is possible to detect very small changes in γ: consider the control parameters $r_0=0.17$ and $c=10^{-7}$, which give the chaotic MMO shown in Figs. 11 and 12. As shown in Fig. 17, when γ is increased by a small amount, the trajectory immediately begins tracing out a large periodic orbit,

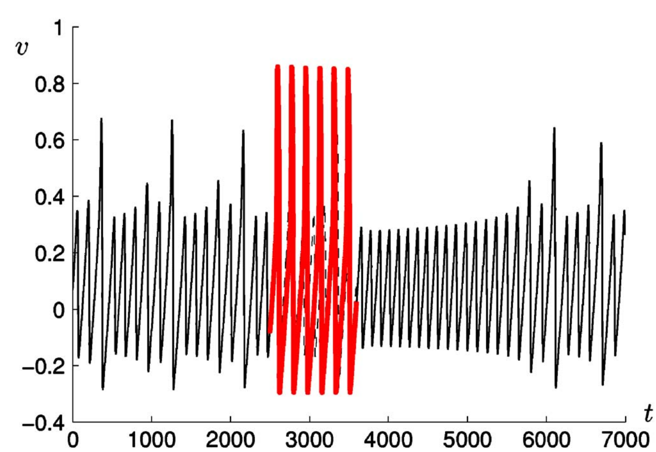

FIG. 17. (Color online) The chaotic system from Fig. 11 with $r_0=0.17$ and $c=10^{-7}$ is able to detect a change (here, an increase) in γ of 3×10^{-4}. As in Fig. 16, the thick, red lines in the middle of the figure show the behavior for the new value of γ, to be compared with the dashed lines which correspond to how the time series would have evolved had γ not changed. After γ returns to 1.0, the system slowly returns to its prior behavior.

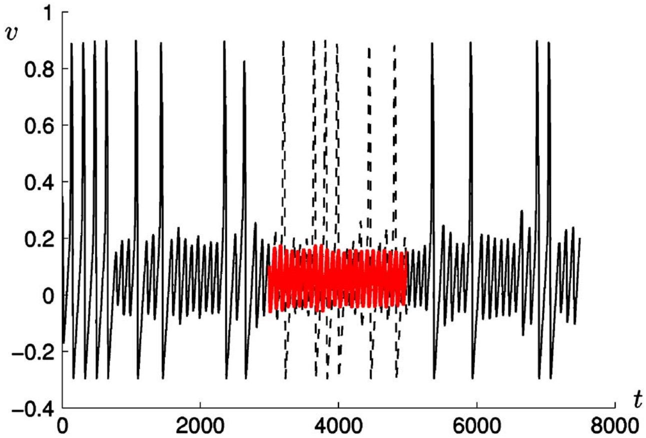

FIG. 18. (Color online) With $r_0=0.17$, $c=10^{-7}$, and a noise strength D of 10^{-7}, the system is able to detect a change (here, a decrease) in γ of 10^{-2}. The thick, red lines in the middle of the figure show the behavior of the system for the new value of γ, to be compared with the dashed lines which correspond to how the time series would have evolved had γ not changed.

which can be easily distinguished from the chaotic MMO. When γ returns to its original value, the system evolves back to chaotic MMO behavior.

Finally, this setup can be used to detect small changes in γ even when the control parameters do not give the maximal canard, and when small noise is present: see Fig. 18 for results with the same control parameters as in Fig. 17, but with noise added. Simulations (not shown) confirm the expected result that when the noise strength is made larger, the size of changes in γ that such a sensor can reliably detect is reduced.

If γ remains at its new value, the control, which always remains on, will cause the system to eventually evolve to the canard regime for the new parameter value. The sensor will then be ready to detect a subsequent change to the parameter value. If this is desired, it might be beneficial to use the adaptive method as shown in Fig. 14 to more rapidly converge to the new canard regime.

VI. CONCLUSION

We have demonstrated a novel technique for controlling the FHN model to be in the canard regime. With the addition of a differential equation regulating the parameter I, so that I now acts as a slow control variable, the model self-tunes to give canardlike orbits. Indeed, when properly tuned, our continuous, memoryless method produces repeated maximal canard trajectories. MMOs, including chaotic trajectories, were observed for suboptimal control setups. While our method can relocate the precise canard region when one of the parameters in the FHN model changes, it can only find the general vicinity of the canard region when subjected to continuous white noise. Furthermore, we demonstrated that a sensor tuned with such control could detect tiny changes to the operating parameters of the system without the hysteresis issues associated with operating at a subcritical Hopf bifurcation. We note that this control strategy will not stabilize unstable canards; for example, on a branch of periodic orbits arising from a subcritical Hopf bifurcation.[21]

In future work, several enhancements to the controller could prove beneficial. Adding an integral term to Eq. (10) could enable the system to more quickly locate the canard orbit when initialized far from the canard region. Adding damping might achieve a similar result and reduce the prevalence of MMOs by shrinking the oscillations in I for larger values of c. Several changes would be necessary to counteract continuous white noise, but a controller that estimated the location of M_U and reduced deviations away from that manifold might prove successful. It would also be interesting to investigate generalizing this control strategy for higher dimensional systems exhibiting canards, using a control cylinder with axis along the fold-line or a hypersphere.

ACKNOWLEDGMENTS

We thank the referees for thoughtful suggestions for improving this paper. We thank the National Science Foundation (Grant No. NSF-0547606) for supporting this research. J.M. was also supported by an Alfred P. Sloan Research Fellowship in Mathematics.

[1]J.-L. Callot, F. Diener, and M. Diener, C. R. Acad. Sci., Ser. I: Math. **286**, 1059 (1978).
[2]E. Benoit, J.-L. Callot, F. Diener, and M. Diener, Collect. Math. **32**, 37 (1981).
[3]W. Eckhaus, Lect. Notes Math. **985**, 449 (1983).
[4]S. M. Baer and T. Erneux, SIAM J. Appl. Math. **46**, 721 (1986).
[5]V. Gáspár and K. Showalter, J. Phys. Chem. **94**, 4973 (1990).
[6]B. Peng, V. Gáspár, and K. Showalter, Philos. Trans. R. Soc. London, Ser. A **337**, 275 (1991).
[7]M. Brøns and K. Bar-Eli, J. Phys. Chem. **95**, 8706 (1991).
[8]S. M. Baer and T. Erneux, SIAM J. Appl. Math. **52**, 1651 (1992).
[9]M. Brøns and K. Bar-Eli, Proc. R. Soc. London, Ser. A **445**, 305 (1994).
[10]F. Dumortier and R. Roussarie, Mem. Am. Math. Soc. **121**, 1 (1996).
[11]M. Krupa and P. Szmolyan, SIAM J. Math. Anal. **33**, 286 (2001).
[12]M. Krupa and P. Szmolyan, J. Differ. Equations **174**, 312 (2001).
[13]S. Schuster and M. Marhl, J. Biol. Syst. **9**, 291 (2001).
[14]V. A. Makarov, V. I. Nekorkin, and M. G. Velarde, Phys. Rev. Lett. **86**, 3431 (2001).
[15]J. Moehlis, J. Nonlinear Sci. **12**, 319 (2002).
[16]K. Bold, C. Edwards, J. Guckenheimer, S. Guharay, K. Hoffman, J. Hubbard, R. Oliva, and W. Weckesser, SIAM J. Appl. Dyn. Syst. **2**, 570 (2003).
[17]H. G. Rotstein, N. Kopell, A. M. Zhabotinsky, and I. R. Epstein, J. Chem. Phys. **119**, 8824 (2003).
[18]F. Marino, G. Catalán, P. Sánchez, S. Balle, and O. Piro, Phys. Rev. Lett. **92**, 073901 (2004).
[19]M. Brøns, Proc. R. Soc. London, Ser. A **461**, 2289 (2005).
[20]M. Wechselberger, SIAM J. Appl. Dyn. Syst. **4**, 101 (2005).
[21]J. Moehlis, J. Math. Biol. **52**, 141 (2006).
[22]F. Marino, F. Mari, S. Balle, and O. Piro, Phys. Rev. Lett. **98**, 074104 (2007).
[23]L. Moreau and E. Sontag, Phys. Rev. E **68**, 020901 (2003).
[24]V. Petrov, S. K. Scott, and K. Showalter, J. Chem. Phys. **97**, 6191 (1992).
[25]M. T. M. Koper, Physica D **80**, 72 (1995).
[26]I. R. Epstein and K. Showalter, J. Phys. Chem. **100**, 13132 (1996).
[27]A. Milik, P. Szmolyan, H. Löffelmann, and E. Gröller, Int. J. Bifurcation Chaos Appl. Sci. Eng. **8**, 505 (1998).
[28]J. Drover, J. Rubin, J. Su, and B. Ermentrout, SIAM J. Appl. Math. **65**, 69 (2004).
[29]G. S. Medvedev and J. E. Cisternas, Physica D **194**, 333 (2004).
[30]R. FitzHugh, Biophys. J. **1**, 445 (1961).
[31]J. Nagumo, S. Arimoto, and S. Yoshizawa, Proc. IRE **50**, 20612070 (1962).
[32]J. Keener and J. Sneyd, *Mathematical Physiology* (Springer, New York, 1998).
[33]M. Brøns, IMACS Transactions on Scientific Computing '88, 12th IMACS World Congress, Paris, 1989, Vol. 1.1, p. 297.

[34]N. Fenichel, Indiana Univ. Math. J. **21**, 193 (1971).
[35]N. Fenichel, J. Differ. Equations **31**, 53 (1979).
[36]S. Wiggins, *Normally Hyperbolic Invariant Manifolds in Dynamical Systems* (Springer, New York, 1994).
[37]J. L. Hudson, M. Hart, and D. Marino, J. Chem. Phys. **71**, 1601 (1979).
[38]M. Schnell and F. N. Albahadily, J. Chem. Phys. **90**, 822 (1989).
[39]R. L. Honeycutt, Phys. Rev. A **45**, 604 (1992).